Atmospheric and Climate Sciences, 2024, 14, 101-117
https://www.scirp.org/journal/acs
ISSN Online: 2160-0422
ISSN Print: 2160-0414

Preliminary Model Study for Forecasting a Hot Weather Process in Guangdong Province Using CMA-TRAMS

Wenfan Wang[1], Jiemin Zhan[1], Dehui Chen[2], Zitong Chen[2], Yanxia Zhang[2], Qing Fan[1*], Guangfeng Dai[2], Yingying Luo[1], Aifen Ye[2]

[1]Department of Applied Mechanics and Engineering, Shenzhen Campus of Sun Yat-sen University, Shenzhen, Guangdong, China
[2]Guangzhou Institute of Tropical and Marine Meteorology/Guangdong Provincial Key Laboratory of Regional Numerical Weather Prediction, CMA, Guangzhou, China
Email: *fanqo@126.com

How to cite this paper: Wang, W.F., Zhan, J.M., Chen, D.H., Chen, Z.T., Zhang, Y.X., Fan, Q., Dai, G.F., Luo, Y.Y. and Ye, A.F. (2024) Preliminary Model Study for Forecasting a Hot Weather Process in Guangdong Province Using CMA-TRAMS. *Atmospheric and Climate Sciences*, **14**, 101-117.
https://doi.org/10.4236/acs.2024.141006

Received: November 23, 2023
Accepted: January 14, 2024
Published: January 17, 2024

Abstract

In this paper, the CMA-TRAMS tropical high-resolution system was used to forecast a typical hot weather process in Guangdong, China with different horizontal resolutions and surface coverage. The results of resolutions of 0.02˚ and 0.06˚ were presented with the same surface coverage of the GlobeLand30 V2020, companies with the results of resolution 0.02˚ with the USGS global surface coverage. The results showed that, on the overall assessment the 2 km model performed better in forecasting 2 m temperature, while the 6 km model was more accurate in predicting 10 m wind speed. In the evaluation of representative stations, the 2 km model performed better in forecasting 2 m temperature and 2 m relative humidity at the coastal stations, and the 2 km model was also better in forecasting 2 m pressure at the representative stations. However, the 6 km model performed better in forecasting 10 m wind speed at the representative stations. Furthermore, the 2 km model, owing to its higher horizontal resolution, presented a more detailed stratification of various meteorological field maps, allowing for a more pronounced simulation of local meteorological element variations. And the use of the surface coverage data of the GlobeLand30 V2020 improved the forecasting of 2 m temperature, and 10 m wind speed compared to the USGS surface coverage data.

Keywords

High-Resolution Numerical Model, CMA-TRAMS Model, Test Evaluation, Surface Coverage, Numerical Simulation

1. Introduction

In the context of global warming, the occurrence of extreme weather events has become more frequent. Predicting these events in advance using numerical weather models is crucial for the safety of human life and property. The meteorological industry worldwide focuses on researching and improving the utilization of these models. With advancements in computer technology and the availability of meteorological data, the accuracy of numerical weather prediction has significantly improved.

Moreover, there has been a gradual improvement in the resolution of global numerical weather prediction models, enhancing their performance in forecasting meteorological elements [1]. The global model developed by the ECMWF (European Centre for Medium-Range Weather Forecasts) now has a horizontal grid distance of less than 10 km, leading to significant improvements in temporal and spatial resolution. This advancement has greatly contributed to the progress of global weather forecasting operations. Furthermore, the development of regional numerical models for small and medium-scale operational weather prediction has been accelerated by utilizing the high-resolution background field of the global model. In recent years, there has been rapid development in high-resolution regional numerical models, with the operational application of kilometer-scale models. Several countries have established regional numerical weather prediction systems with horizontal grid spacing ranging from 1 to 3 km. For instance, the UK Meteorological Office has implemented a 1.5 km high-resolution regional model and a 2.2 km regional ensemble forecast system based on the unified model [2]. Meteo France has developed a 1.3 km high-resolution regional model and a 2.5 km regional ensemble forecast system. Similarly, the German Meteorological Office has established a 2.8 km high-resolution regional model and a 2.8 km regional ensemble forecast system.

Many scholars have been exploring the development of high-resolution regional numerical models to forecast regional weather processes and evaluate their performance. Lean *et al.* [3] conducted simulations using various high-resolution numerical prediction models with a horizontal grid spacing of 12 km, 4 km, and 2 km to test summer convective precipitation events in the UK. They found that the 4 km and 1 km models provided precipitation closer to reality and performed better than the 16 km model for precipitation threshold prediction, but had poor representation in the early stage of simulation and prediction. Gao *et al.* [4] used the WRF (Weather Research Forecast) numerical forecasting model with a 4 km horizontal grid spacing to simulate extreme heat waves and precipitation events in the eastern United States. They found that the high-resolution model significantly improved the forecasting of extreme weather events. Latt *et al.* [5] found that the high-resolution COSMO-CLM (Continuous Consortium for Scale Modeling in Climate Mode) model simulation portrayed the main characteristics of regional winds, with the regional climate numerical model per-

forming better in regions with complex topography. For certain extreme weather conditions and regions with complex terrain, higher model resolution leads to some improvement in simulation results. However, during general weather processes, regional high-resolution models exhibit satisfactory simulation performance. Chen *et al.* [6] combined the WRF model with a 1 km horizontal resolution and the UCM (Urban Canopy Model) to simulate a prolonged heatwave in Hangzhou, China. The high-resolution model reasonably simulated the spatial and temporal characteristics of meteorological elements during the heatwave. De Meij *et al.* [7] incorporated the latest surface coverage dataset into the WRF model with a 5 km horizontal resolution to investigate the effects on meteorological conditions in summer and winter. Based on GRAPES (Global and Regional Assimilation and Prediction System), the CMA-TRAMS tropical high-resolution model was developed at the Guangzhou Institute of Tropical and Marine Meteorology, Guangzhou, China. Chen *et al.* [8] tested its 3.0 version with a real-time application showing its advantages in forecasting fine rain, heavy rain, surface elements, etc. Poschlod *et al.* [9] used three high-resolution regional numerical models to generate daily precipitation regression levels and evaluated their forecasting performance by comparing them with observed data. The results showed that the three high-resolution models provided relatively reliable precipitation predictions. Mohanty *et al.* [10] simulated the prediction of the tropical cyclone Fani over the Bay of Bengal using two high-resolution numerical prediction models, which accurately predicted the storm's location and intensity. Lin *et al.* [11] assessed the forecasting capabilities of regional high-resolution numerical models for meteorological elements such as precipitation, surface temperature, and wind fields in the South China region. The model horizontal resolutions considered were 1 km and 3 km. The results indicate that both high-resolution models can effectively simulate this weather event, with each demonstrating advantages in forecasting various meteorological elements.

Guangdong Province, the largest economic province in China, houses the Pearl River Delta urban agglomeration, one of the three largest megacities in the country. Its rapid population and economic growth have accelerated urbanization, with an urbanization rate of 71.45% by the end of 2020 [12]. As urbanization continues, the region's climate is gradually warming, leading to frequent and prolonged hot weather events in summer [13]. Understanding the spatial and temporal distribution characteristics of errors in the regional high-resolution numerical weather prediction model in Guangdong Province is crucial for improving forecast accuracy and aiding forecasters in assessing model performance. This study focuses on evaluating the CMA-TRAMS model's forecasts with different horizontal resolutions and surface coverages. In order to justify the choice of input data and the parameters of the CMA-TRAMS model, the results were assessed by mean absolute and root mean square errors of 2 m temperature and 10 m speed wind speed predictions, and comparison between the results of different resolutions and surface coverages were performed to check their effects.

2. Methodology of Information and Experimental Design

2.1. Model Setup and Data Description

CMA-TRAMS was used in this paper to test three cases with different horizontal resolutions and/or surface coverages. The first case referred to hereafter as the "2 km-20 model" has a calculating region starting at the latitude of 10˚N and longitude of 102˚E with a horizontal resolution of 0.02˚. The horizontal grid dimensions are 1250 × 1000. The second, referred to as the "6 km-20 model", has a horizontal resolution of 0.06˚, starting at a latitude of 10˚N and a longitude of 100˚E. The horizontal grid dimensions are 382 × 332. The two cases both used the 2020 GlobeLand30 global surface coverage, in contrast to the third case, in which the US Geological Survey (USGS) global surface coverage was used, referred to as the "USGS model" having the same calculating region and horizontal resolution with the "2 km-USGS model". All three cases employ the same parameterization schemes, including the WSM6 (Single-Moment 6-Class Microphysics scheme) cloud microphysics, RRTM (Rapid Radiative Transfer Model) longwave and shortwave radiation, MRF boundary layer, SLAB heat diffusion, and SAS (Simple Arakawa-Schubert scheme) cumulus cloud schemes. The vertical direction is divided into 65 layers, with the top of the model reaching a height of 30,000 m. The integration time steps were set to 30 s, 50 s, and 30 s respectively for the three cases.

The model utilizes the ECMWF 0.125˚ forecast information every 6 hours for generating initial and boundary conditions. The model simulation was performed at 2020070500 (UTC, the same as below), with the top layer extending up to a maximum height of 20,000 m. The simulation time spans from 2020070500 to 2020070700 for a duration of 48 hours. The observational data used in this study were sourced from Guangdong Province, specifically hourly observations from national and regional automatic meteorological stations, including temperature, wind speed, relative humidity, and other meteorological elements.

2.2. Introduction and Processing of Surface Cover Type Data

This paper incorporated the 2020 GlobeLand30 global surface coverage data into a high-resolution regional numerical model for a comparative analysis with the default USGS surface coverage data. The aim is to investigate the impact of different surface coverage datasets on the simulation and prediction capabilities of the high-resolution model.

The GlobeLand30 surface coverage data adopts the WGS-84 coordinate system and the UTM projection method, covering a vast land area from 80˚ north to 80˚ south latitude. With a spatial resolution of 30 meters, GlobeLand30 data has been extensively analyzed and evaluated by numerous scholars, consistently demonstrating high accuracy across both temporal and spatial scales [14] [15]. On the other hand, the USGS global surface coverage dataset is derived from the 1-kilometer AVHRR (Advanced Very High-resolution Radiometer) data collected by USGS from 1992 to 1993. The data was processed using unsupervised image classification methods. It is also based on the WGS-84 coordinate system

and UTM projection but with a resolution of 1 kilometer.

To successfully integrate the GlobeLand30 data into the model, the following specific processing steps were implemented:

1) Download the 2020 GlobeLand30 surface coverage data for the experimental simulation area addressed in this paper.

2) Utilize GIS ArcGIS software to perform secondary development on multiple images, stitching them together to obtain the 2020 surface coverage data for the study area.

3) Reclassify and map the data into the 24 classes defined by USGS.

4) Use the GDAL spatial data conversion library to convert the obtained surface coverage data from TIF format to binary format for static data storage. Additionally, modify the index file to reflect the appropriate data storage format, range, and resolution.

5) Adjust the file paths in the model-related files to ensure easy access to the data during the compilation and execution stages of the model.

2.3. Test Methods

The weather element test was conducted to assess the model's reliability in simulating weather processes and evaluate its performance with Mean Absolute Error (MAE), Root Mean Square Error (RMSE) and Absolute Error (AE) statistical measures for 2 m temperature, 10 m wind speed, 2 m pressure, and 2 m relative humidity in this paper. The statistical formula is as follows:

$$\mathrm{MAE} = \frac{1}{n}\sum_{i=1}^{n}\left|\hat{x}_i - x_i\right| \tag{1}$$

$$\mathrm{RMSE} = \sqrt{\frac{1}{n}\sum_{i=1}^{n}\left(\hat{x}_i - x_i\right)^2} \tag{2}$$

$$\mathrm{AE} = \left|\hat{y}_i - y_i\right| \tag{3}$$

where x_i: simulated values on the model grid points; $\hat{x}_i$: station observations obtained by interpolation; n: total number of weather stations, y_i: simulated values for the site; $\hat{y}_i$: observed values for the site.

To facilitate the evaluation test, the station observation data was interpolated to the model grid points using bilinear interpolation. The simulated values at each grid point were then compared with the corresponding observed values. Absolute errors at representative sites were calculated from the simulated values and the observed values at representative sites. The calculating region and the station locations (Chaozhou, Huadu, Shaoguan, and Zhanjiang) were presented in **Figure 1**, in which the surface coverage of the region was also presented.

2.4. Experimental Design

This paper designed three cases of experiments, namely the aforementioned "2 km-20 model", "6 km-20 model" and "2 km-USGS model". The first case had a horizontal resolution of 0.02˚ with the 2020 GlobeLand30 global surface coverage data, the second resolution of 0.06˚ with the 2020 GlobeLand30 global surface

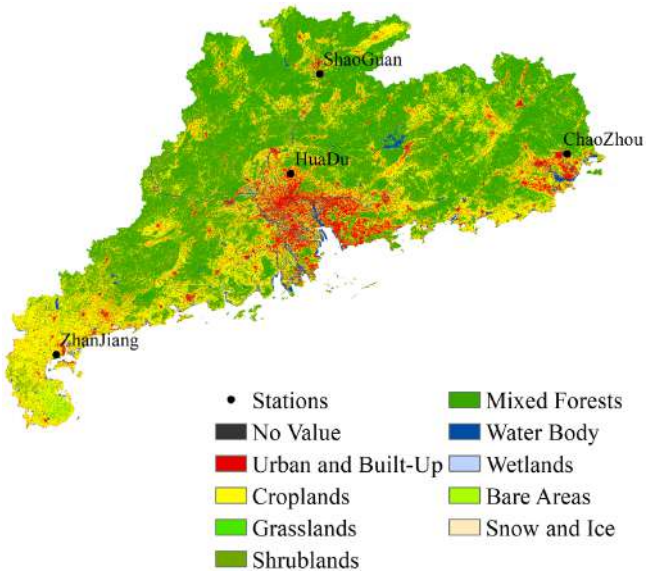

Figure 1. Overview of GlobeLand30 surface coverage and distribution of representative stations in Guangdong Province in 2020.

coverage data and the third resolution of 0.02˚ with the USGS global surface coverage data. All three cases had the same parameterization schemes and were used to simulate the same weather process.

3. The Significance of Weather Description and Time Period Selection for the Simulation Period

In July 2020, Guangdong Province experienced an unusually high average temperature, 1.5˚C higher than the historical average for the same period. The average temperature in July reached a record high of 30˚C since meteorological records began. From July 5 to 7, 2020, the province encountered a three-day heatwave. This simulation period represents a typical and extensive hot weather process in Guangdong Province. Evaluating the performance of the regional high-resolution weather prediction numerical model during this hot weather period provides valuable insights into its effectiveness and offers guidance for improving refined weather prediction in the region. It also assists model developers in identifying areas for technical enhancement.

4. Analysis of Results

4.1. Overall Assessment of 2 m Temperature and 10 m Wind Speed Forecasts

To justify the choice of the schemes and parameters used in CMA-TRAMS in this paper. the mean absolute error (MAE) and root mean square error (RMSE) of the 2 m temperature and 10 m wind speed for 6 h, 12 h, 18 h, and 24 h in the Guangdong province region were presented in Figure 2. For the three models, the MAE and the RMSE of the 2 m temperature fell below 3.1˚C and 3.6˚C, respectively. And the MAE and the RMSE of the 10 m wind speed fell below 2.6

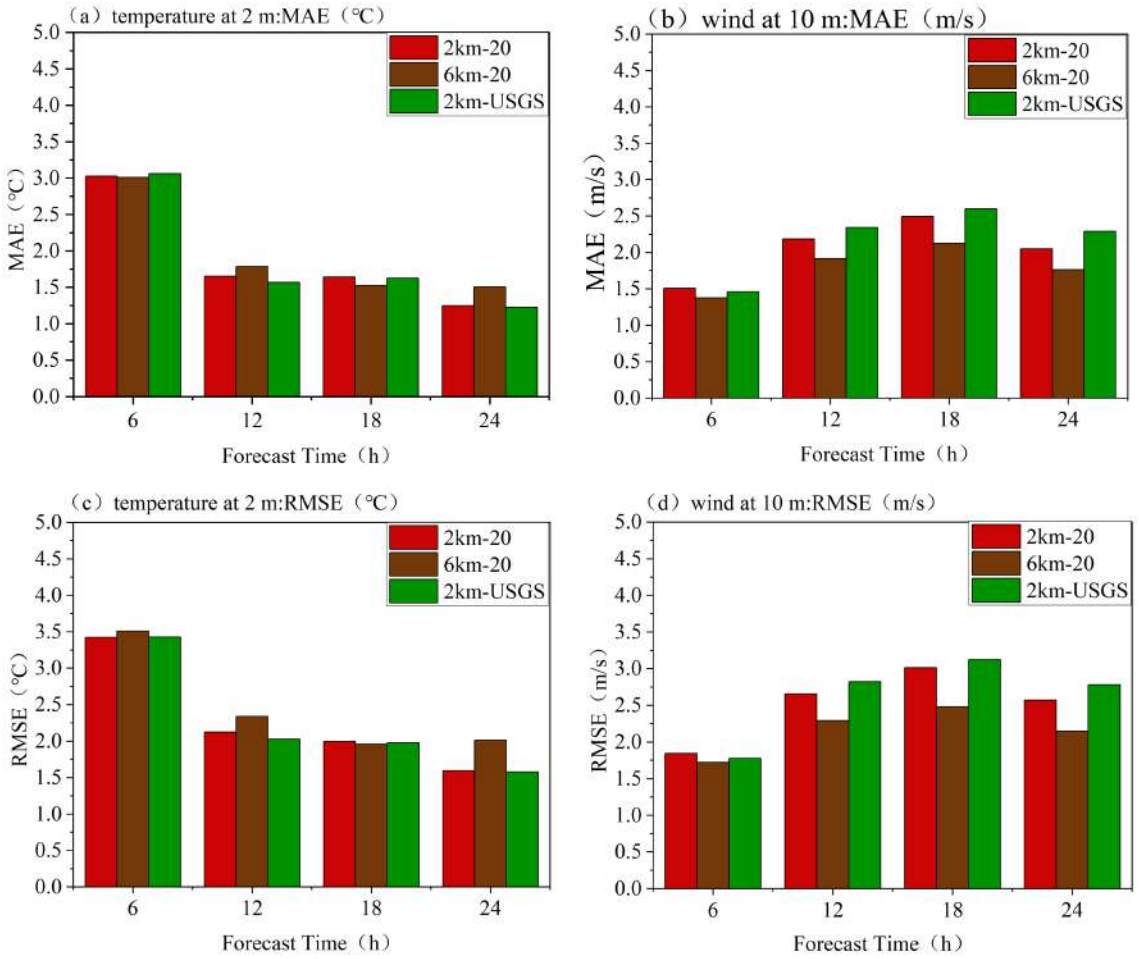

Figure 2. Presents the mean absolute errors ((a), (b)) and root-mean-square errors ((c), (d)) of the 2 m temperature ((a), (c)) and 10 m wind speed ((b), (d)) for both the 2 km and 6 km models.

m/s and 3.2 m/s respectively. These errors fell within the acceptable range, indicating the relative reliability of the aforementioned models for forecasting the 2 m temperature and 10 m wind speed.

It also can be seen in Figure 2, there is no significant difference in the MAE and RMSE between the 2 km-20 and the 2 km-USGS models for the 2 m temperature forecast that was generally slightly better predicted when compared with the results with the 6 km model, particularly for the 12 h and 24 h forecasts. The average MAE was 1.89 and the average RMSE was 2.28 for the 2 km models, compared to an average MAE of 1.96 and an average RMSE of 2.46 for the 6 km model.

Regarding the forecast of the 10 m wind speed, the 2 km-20 model slightly outperforms the 2 km-USGS model at 12 h, 18 h, and 24 h. However, the 6 km model demonstrates significantly better forecasting performance than the 2 km models, similar to the results obtained by Lin *et al.* [11].

4.2. Characterization of Stations

In addition to the overall assessment of the three models, four national stations were chosen in Guangdong province, namely ChaoZhou, HuaDu, Shaoguan and

Zhanjiang (the locations were shown in Figure 1), whose observation results were used to compare with the predictions. The absolute errors (AEs) between the observed values and the forecast results of the 2 km model and the 6 km model, obtaining the AE time series for each meteorological element over a 24-hour period, are shown in Figures 3-6.

4.2.1. 2 m Temperature

Figure 3 displays the time series of AEs for the 2 m temperature of the 2 km-20 model and the 6 km-20 model at the four stations. Overall, the maximum absolute error for both models does not exceed 5˚C, remaining reasonable for temperature forecasting. Analyzing the time series of absolute errors for 2 m temperature, it was evident that the HuaDu and Shaoguan stations exhibit significant fluctuations in forecast accuracy for both models. Comparing the 2 m temperature AE time series across the four stations, it became clear that the 2 km-20 model provides superior forecasts at Chaozhou and Zhanjiang stations compared to the 6 km-20 model. The absolute errors for the 2 km-20 model were smaller, and the AE curves were smoother during the 0512-0524 time period. The average absolute error for 24-hour 2 m temperature at Chaozhou station was 2.05˚C for the 2 km-20 model and 2.34˚C for the 6 km-20 model. Similarly, the average absolute error for 24-hour 2 m temperature at Zhanjiang station was 1.15˚C for the 2 km-20 model and 1.67˚C for the 6 km-20 model. Thus, it can be concluded that the 2 km-20 model performed better than the 6 km-20 model for coastal stations, particularly regarding 2 m temperature forecasts.

4.2.2. 10 m Wind Speed

Figure 4 displays the time series of AEs for the 10 m wind of the 2 km-20 model and the 6 km-20 model at the four stations. Overall, the maximum absolute error for both models does not exceed 4 m/s, which is still reasonable for wind speed forecasting. Comparing the AE time series for 10 m wind speed at the four stations between the two models, it was apparent that the 2 km-20 model

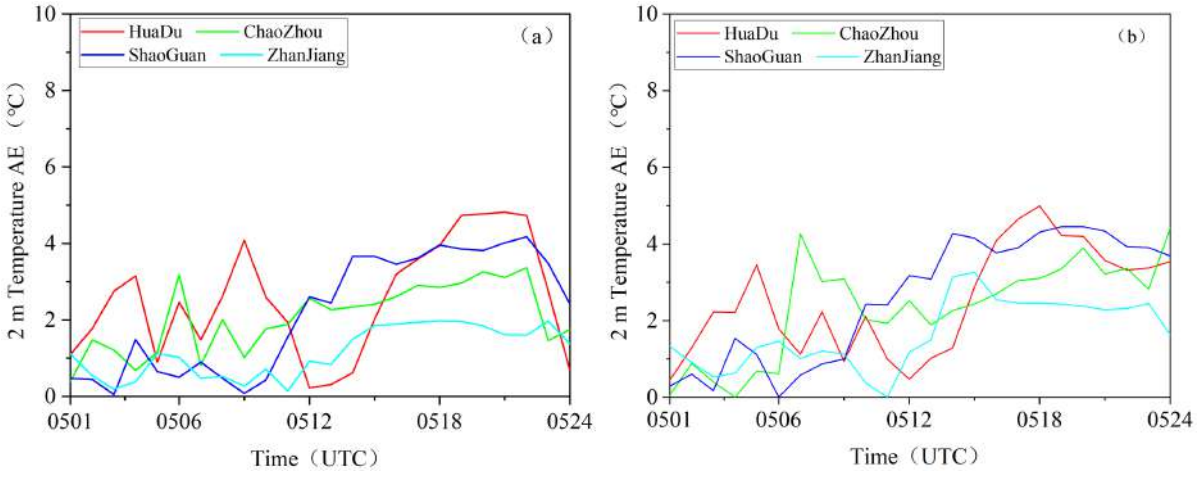

Figure 3. Time series of absolute errors (AEs) in 2 m temperature for four stations in the 2 km-20 model (a) and the 6 km-20 model (b).

exhibits larger fluctuations and higher absolute errors compared to the 6 km-20 model. This aligned with the previous findings that the MAE and RMSE for 10 m wind speed in the 2 km-20 model were larger than those in the 6 km-20 model for the Guangdong province region. In the 2 km-20 model, the MAE for 24-hour 10 m wind speed at HuaDu, Chaozhou, Shaoguan, and Zhanjiang stations were 1.04 m/s, 1.29 m/s, 1.30 m/s, and 1.30 m/s, respectively. In the 6 km-20 model, the MAE for 24-hour 10 m wind speed at HuaDu, Chaozhou, Shaoguan, and Zhanjiang stations were 0.65 m/s, 0.89 m/s, 1.13 m/s, and 1.07 m/s, respectively".

4.2.3. 2 m Pressure

Figure 5 displays the time series of AEs for the 2 m pressure of the 2 km-20 model and the 6 km-20 model at the four stations. By comparing the time series of AE in 2 m pressure at the two sets of test stations, it became evident that the 2 km-20 model performs better than the 6 km-20 model in forecasting 2 m pressure overall, particularly at the Chaozhou and Shaoguan stations. In the 2

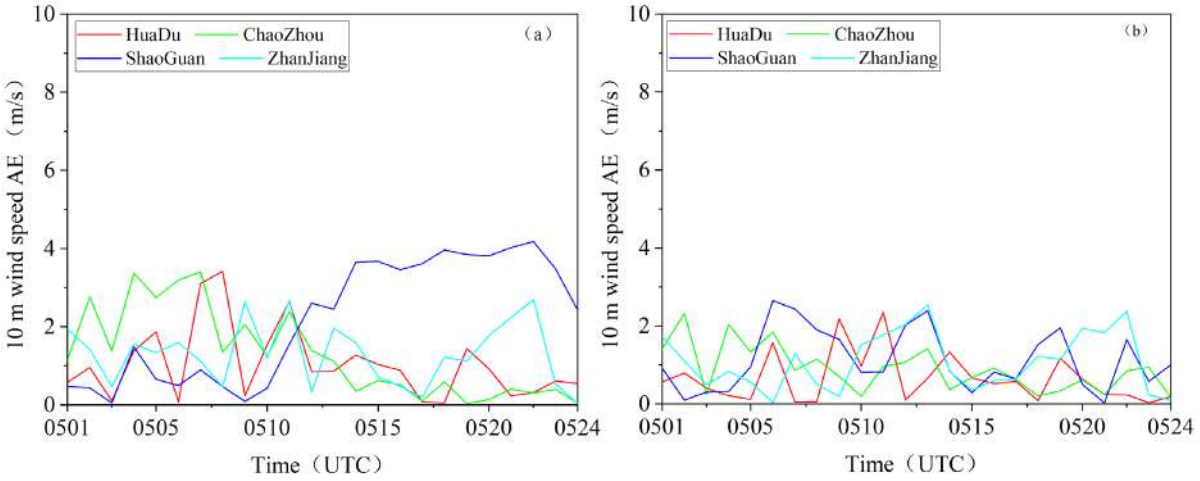

Figure 4. Time series of absolute errors (AEs) in 10 m wind speed for four stations in the 2 km-20 model (a) and the 6 km-20 model (b).

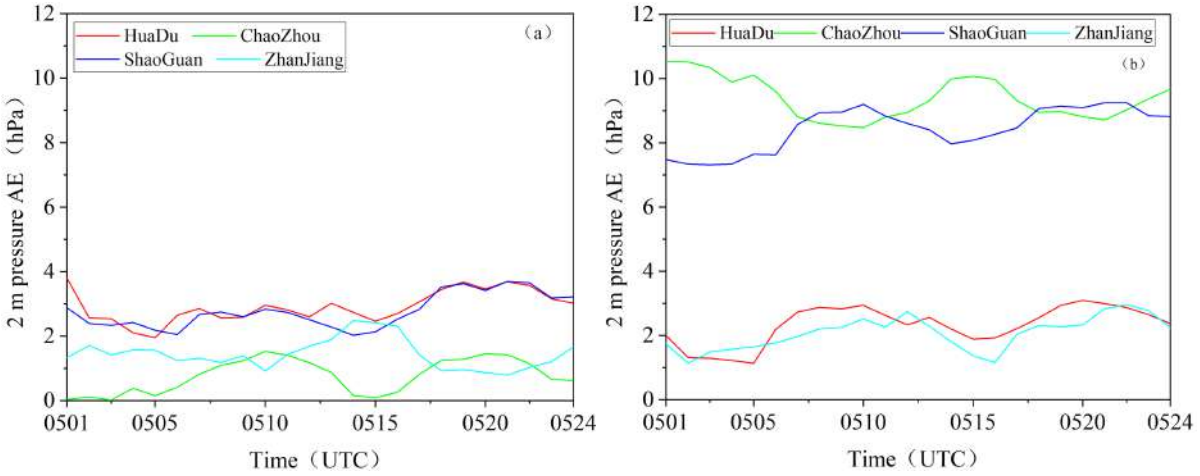

Figure 5. Time series of absolute errors (AEs) in 2 m pressure for four stations in the 2 km-20 model (a) and the 6 km-20 model (b).

km-20 model, the 24-hour average absolute errors of 2 m pressure at HuaDu, Chaozhou, Shaoguan, and Zhanjiang stations were as follows: 2.9 hPa, 0.76 hPa, 2.76 hPa, and 1.43 hPa, respectively. On the other hand, in the 6 km-20 model, the 24-hour average absolute errors of 2 m pressure at the same stations were as follows: 2.32 hPa, 9.39 hPa, 8.44 hPa, and 2.07 hPa, respectively.

4.2.4. 2 m Relative Humidity

Figure 6 displayed the time series of AEs for the 2 m relative humidity of the 2 km-20 model and the 6 km-20 model at the four stations. Analyzing the time series of 2 m relative humidity AEs at the four stations, it was evident that the fluctuations in the time series of 2 m relative humidity absolute errors were more pronounced in the two groups of tests at the HuaDu and Shaoguan stations. For the Chaozhou and Zhanjiang stations, the 2 km-20 model showed smaller absolute errors in 2 m relative humidity compared to the 6 km-20 model, with more noticeable differences during the 0512-0524 time period. In the 2 km-20 model, the 24-hour MAEs of 2 m relative humidity at the Chaozhou and Zhanjiang stations were 7.66% and 4.54%, respectively. On the other hand, in the 6 km-20 model, the 24-hour MAEs of 2 m relative humidity at the same stations were 9.06% and 6.2%, respectively. This difference can be attributed to the fact that 2 m temperature had a greater influence on 2 m relative humidity, and at the Chaozhou and Zhanjiang stations the forecasts of 2 m temperature in the 2 km-20 model during the 0512-0524 time period were better than those in the 6 km-20 model, thus demonstrating better performance in forecasting 2 m relative humidity during that time frame.

4.3. Impact of Different Sets of Surface Coverage Data on Regional High-Resolution Numerical Model Simulations

In order to compare the forecasts of different surface coverage, the results of 2 km-20 and 2 km-USGS models are presented companying observed measures in

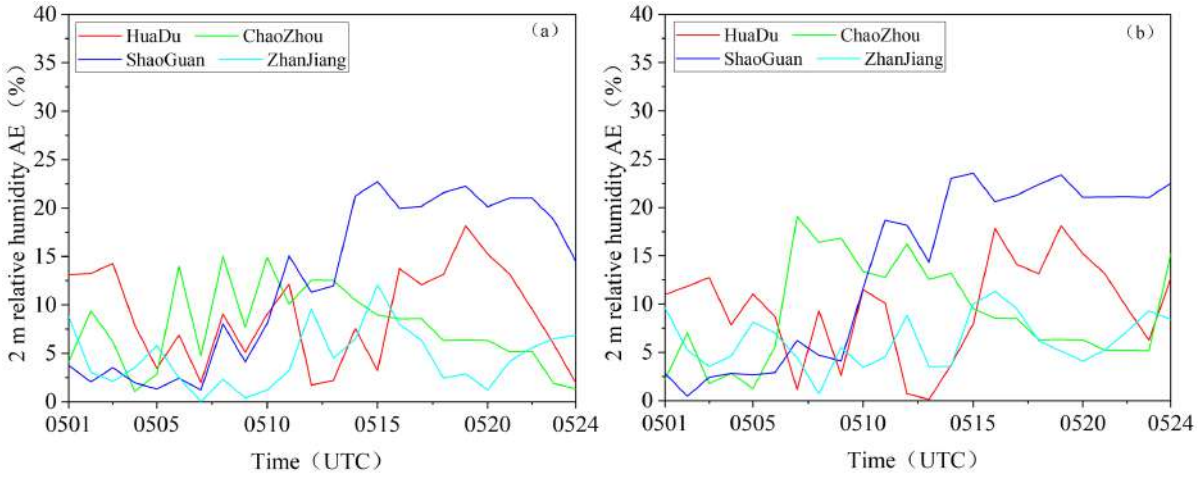

Figure 6. Time series of absolute errors (AEs) in 2 m relative humidity for four stations in the 2 km-20 model (a) and the 6 km-20 model (b).

Figure 7 & Figure 8, in which the surface coverage data of the GlobeLand30 V2020 and the USGS global surface coverage were used respectively.

4.3.1. 2 m Temperature

Figure 7 shows the time series of 2 m temperature for the 2 km-20 and the 2 km-USGS models at four stations. The simulated 2 m temperatures from the high-resolution model under different sets of surface coverage data were compared with the observed values. Overall, the simulated 2 m temperatures at the

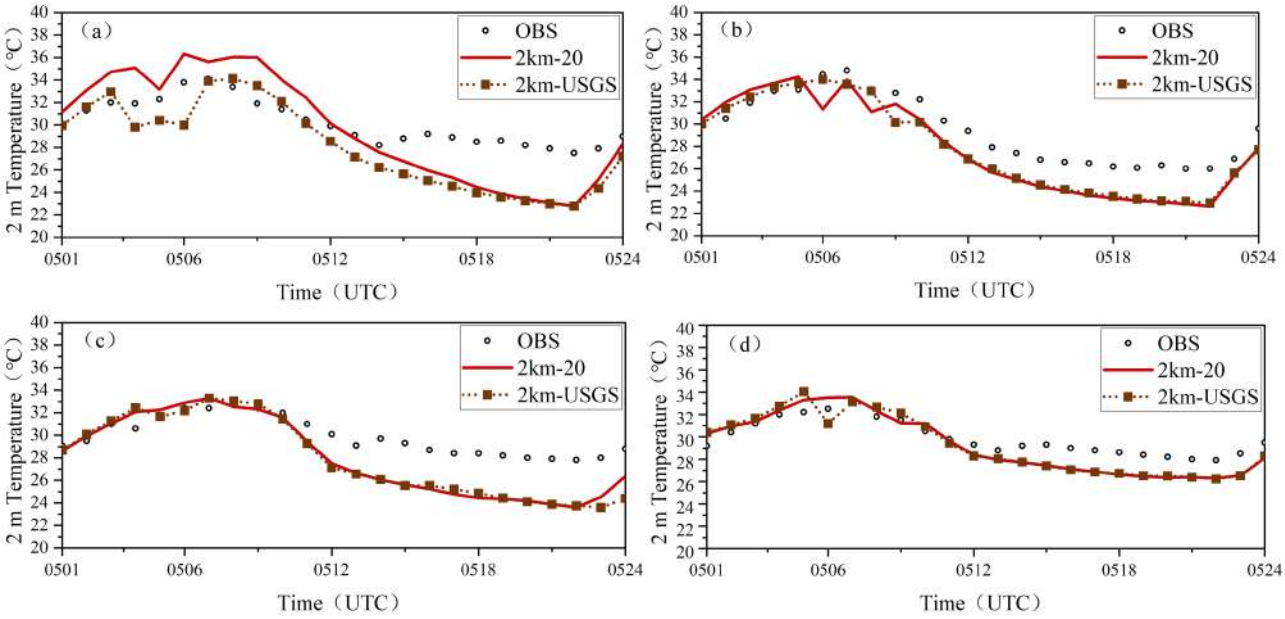

Figure 7. Time series of 2 m temperature of 2 km-20 model and 2 km-USGS model at 4 stations ((a) HuaDu; (b) ChaoZhou; (c) Shaoguan; (d) Zhanjiang).

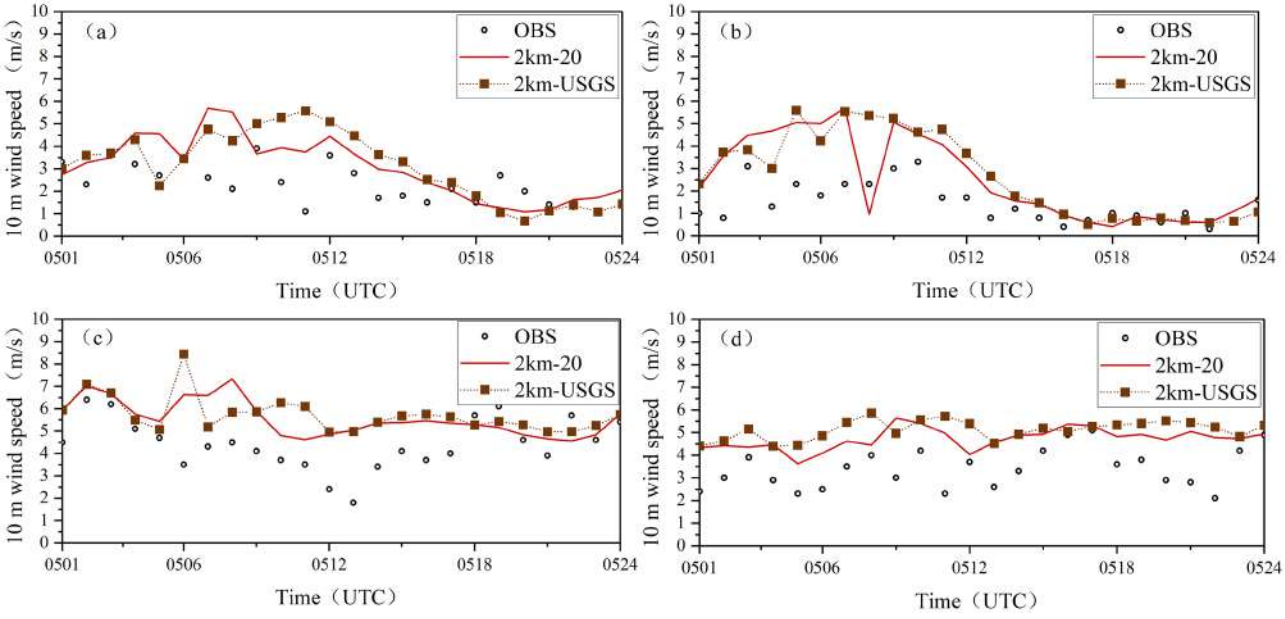

Figure 8. Time series of 10 m wind speed of 2 km-20 model and 2 km-USGS model at 4 stations ((a) HuaDu; (b) ChaoZhou; (c) Shaoguan; (d) Zhanjiang).

four stations for both sets of experiments showed a similar trend compared to the observed values. During the 0512-0524 time period, the simulated temperatures were lower than the measured values, and there was little difference between the two experiments.

For ChaoZhou, Shaoguan, and Zhanjiang stations, the simulated and measured temperatures were in good agreement during the 0512-0524 time period. However, at HuaDu station, the 2 km-20 model showed higher temperatures than the measured values during the high-temperature period, while the 2 km-USGS model showed some simulated values lower than the measured values during the high-temperature period.

4.3.2. 10 m Wind Speed

Figure 8 illustrates the time series of 10 m wind speeds for the 2 km-20 and the 2 km-USGS models at four stations. Similar to the 2 m temperature, the high-resolution model simulated the 10 m wind speed under different surface coverage datasets, and the results were compared with the observed values.

The simulation results of both models were consistent with the observed values, but the simulated values were generally larger than the measured values. In the 2 km-20 model, most of the simulated values were lower than those in the 2 km-USGS model to varying degrees, indicates that the 2 km-20 model showed a slightly better forecast effect on the 10 m wind speed compared to the 2 km-USGS model. This finding aligned with the conclusions mentioned in the previous section.

4.4. Meteorological Field Simulation Analysis

As shown in the previous section, the overall and stational errors did not vary significantly between different models. In order to further compare the performance of the aforementioned three models, the spatial distribution of 2 m temperature and 10 m wind speed were presented in Figure 9 & Figure 10. The results of the 6 km-20 and 2 km-USGS models were compared with that of the 2 km-20 model.

4.4.1. 24-Hour Average Meteorological Field

Figure 9 presented the 24-hour average 2 m temperature field maps, 10 m wind field maps, and 2 m relative humidity field maps for the 2 km-20 model and the 6 km-20 model in Guangdong Province. Overall, the spatial distribution of meteorological elements simulated by the two sets of experiments was generally consistent. However, due to the higher horizontal resolution employed in the 2 km-20 model, its simulation of various meteorological field maps was more detailed in stratification. Based on the 24-hour average 2 m temperature field maps (a) and (b), it can be observed that the 2 km-20 model simulates a range of temperatures above 18˚C that was significantly larger in the Pearl River Delta and Chaoshan regions compared to the 6 km-20 model. Moreover, it was evident that the 2 km-20 model simulates higher high temperatures and lower low temperatures.

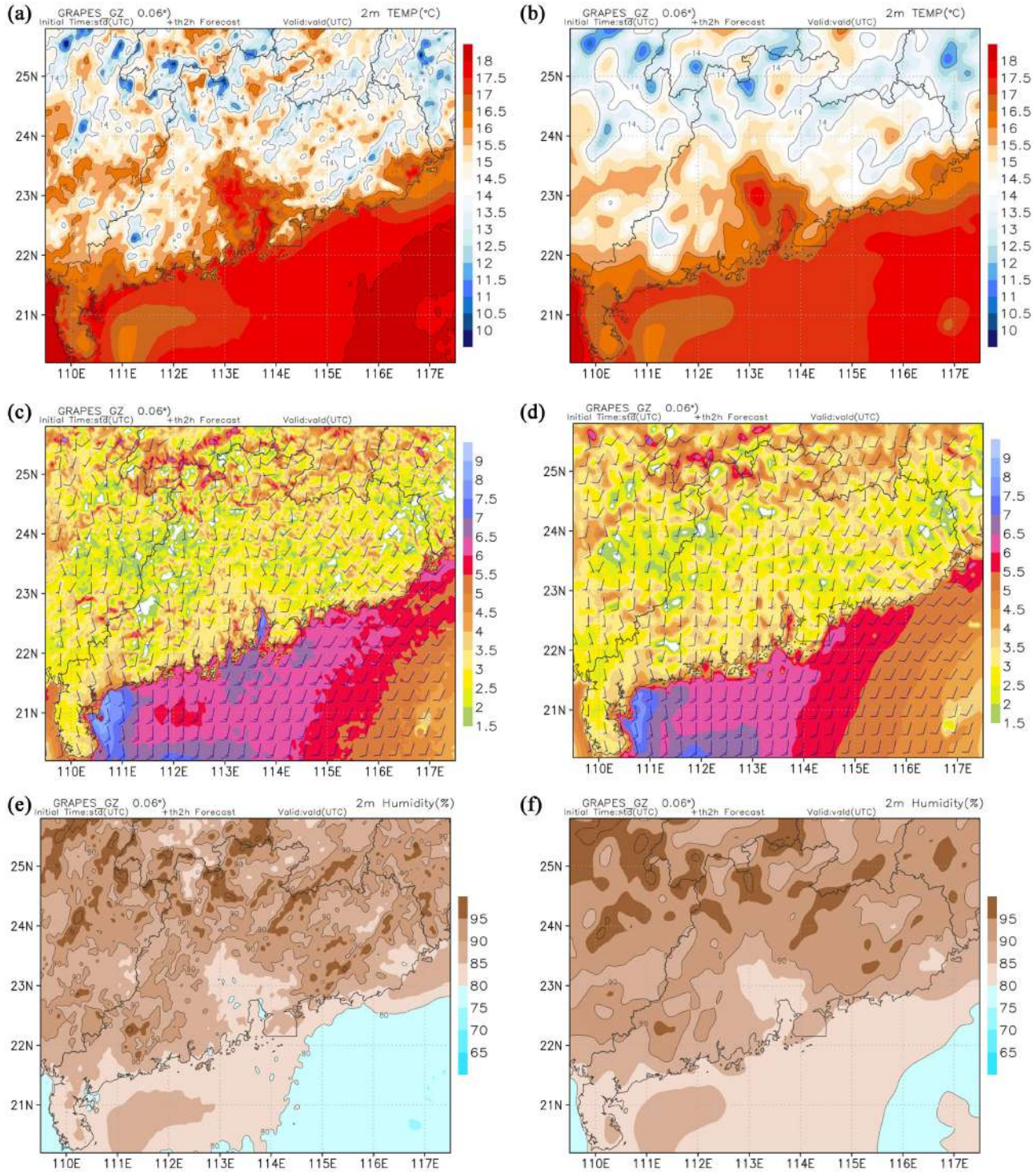

Figure 9. 24-hour averaged 2 m temperature ((a), (b)), 10 m wind speed ((c), (d)), and 2 m relative humidity ((e), (f)) for the 2 km-20 model ((a), (c), (e)) and the 6 km-20 ((b), (d), (f)) model.

Observing the 24-hour average 10 m wind field maps (c) and (d), there were noticeable differences in the depiction of wind speed in local areas between the two sets of experiments. Additionally, there were differences in the description of wind direction changes, with the 2 km-20 model showing more pronounced

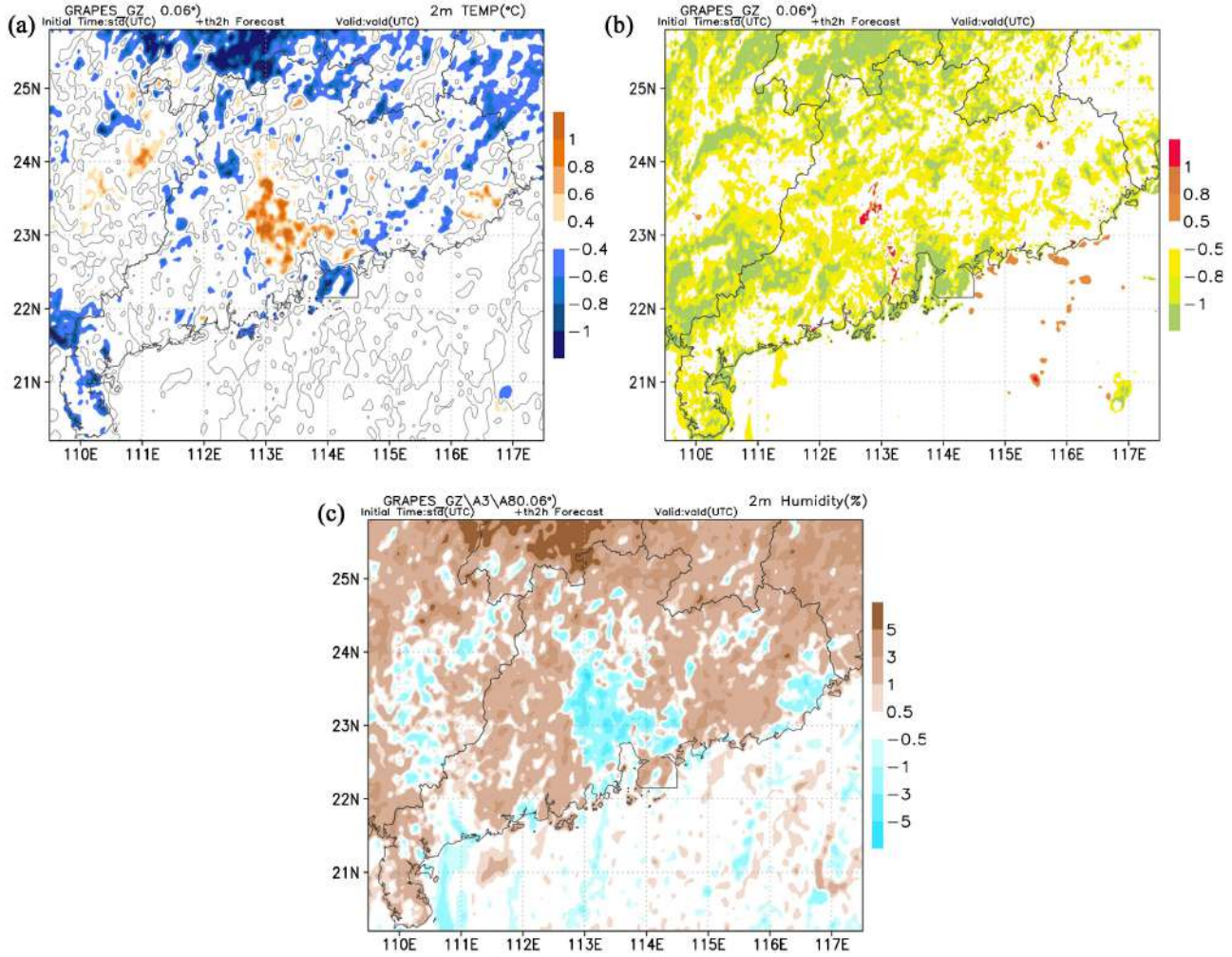

Figure 10. Difference maps of 24-hour average 2 m temperature (a), 10 m wind speed (b), and 2 m relative humidity (c) between the 2 km-20 model and the 2 km-USGS model.

changes in wind direction in the northern part of the Pearl River Delta. As shown in the 24-hour average 2 m relative humidity field maps (e) and (f), due to the influence of 2 m temperature to some extent on 2 m relative humidity, the 2 km-20 model simulated a range of 2 m relative humidity below 85% that was significantly larger in the Pearl River Delta and Chaoshan regions compared to the 6 km-20 model.

4.4.2. 24-Hour Mean Meteorological Field Difference

Figure 10 presented the difference maps of the 24-hour average 2 m temperature, 10 m wind, and 2 m relative humidity fields between the 2 km-20 model and the 2 km-USGS model (the results of the 2 km-20 model minus that of the 2 km-USGS model) in Guangdong Province. From the average 2 m temperature difference map (a) of the two models, it can be inferred that the 2 km-20 model simulates an average 2 m temperature in the Pearl River Delta region that is 0.6˚C - 1˚C higher than that simulated by the 2 km-USGS model, with some local areas even exceeding 1˚C. The possible reason was the significant expansion

of urban underlying surfaces in the Pearl River Delta region, and the land cover used in the 2 km-20 model was closer to the actual conditions, resulting in a higher simulated average 2 m temperature in the Pearl River Delta region.

Observing the difference maps of the average 10 m wind speed (b) for the two models, it was evident that the 10 m wind speed simulated by the 2 km-20 model was generally lower than that of the 2 km-USGS model. As shown in the difference maps of the average 2 m relative humidity (c) for the two models, in the Pearl River Delta region, compared to the 6 km-20 model, the 2 km-20 model simulated significantly lower 2 m relative humidity, to some extent influenced by the 2 m temperature.

5. Conclusions

In this paper, a typical hot weather process encountering a three-day heatwave from July 5 to 7, 2020 in Guangdong province, China was simulated using the CMA-TRAMS tropical high-resolution system with three models varying in the horizontal resolution and/or the surface coverage, referred to as the "2 km-20", "6 km-20" and "2 km-USGS" model. The results of these models were compared based on overall and stational prediction errors and the spatial distribution of temperature, wind speed and relative humidity. The main conclusions are as follows:

1) The simulation results of the three models for the hot weather process were reliable. The overall mean absolute errors and root-mean-square errors of the forecasts for 2 m temperature and 10 m wind speed were within the permissible error range. While the 2 km model outperformed the 6 km model in forecasting 2 m temperature, while the 6 km model performed better in the prediction of 10 m wind speed, similar to the previous study.

2) The 2 km model showed better performance than the 6 km model in forecasting 2 m temperature at coastal stations (Chaozhou and Zhanjiang stations). The AEs of the 2 km model were smaller, and their fluctuations were also smaller during the period of 0512-0524. The 2 km model also outperformed the 6 km model in forecasting 2m relative humidity at coastal stations. However, the 2 km model performed worse than the 6 km model in forecasting 10 m wind speed at all four stations. The 2 km model performed better than the 6 km model in forecasting 2 m pressure at all four stations, especially at Chaozhou and Shaoguan stations.

3) With a different set of surface coverage data, the 2 km-20 model, which corresponded to the 2020 GlobeLand30 surface coverage data closer to the actual surface coverage, performed better in simulating high temperatures at HuaDu station compared to the results of the 2 km-USGS model with the USGS global surface coverage data. The 2 km-20 model also slightly outperformed the 2 km-USGS model in predicting 10 m wind speed at the four stations.

4) By comparing the averaged meteorological field maps of the 2 km model and the 6 km model, it was evident that the 2 km model, with its higher hori-

zontal resolution, exhibited a more detailed stratification in simulating various meteorological fields. It demonstrated a more pronounced simulation of the changes in local meteorological elements. Analyzing the averaged difference field maps of meteorological elements between the 2 km-20 model and the 2 km-USGS model, it can be observed that in the Pearl River Delta region with significant urban expansion, the 2 km-20 model simulated higher average 2 m temperature and noticeably lower average 2 m relative humidity compared to the 2 km-USGS model. In the entire province, the 2 km-20 model generally simulated lower 10 m wind speed than the 2 km-USGS model.

In conclusion, for the hot weather process presented in this paper, the overall performance of the three models differing in horizontal resolutions and/or surface coverage was similar. However, as the 2 km-20 models used higher horizontal resolution and more actual surface coverage data, it outperforms the other two models in local details. This paper focuses on individual hot weather events in Guangdong Province due to the limitation of the model forecast data. The results of the model simulations may be affected by different climatic conditions. To obtain more comprehensive and accurate model performance evaluation results, conducting long-term simulations of different types of case processes in Guangdong Province and analyzing the differences in the results in the future is necessary.

Acknowledgements

This work is supported by Shenzhen Science and Technology Program of China (No. JCYJ20220818102012024).

Conflicts of Interest

The authors declare no conflicts of interest regarding the publication of this paper.

References

[1] Simmons, A.J., Burridge, D.M., Jarraud, M., Girard, C. and Wergen, W. (1989) The ECMWF Medium-Range Prediction Models Development of the Numerical Formulations and the Impact of Increased Resolution. *Meteorology and Atmospheric Physics*, **40**, 28-60. https://doi.org/10.1007/BF01027467

[2] Staniforth, A., White, A., Wood, N., *et al.* (2006) Unified Model Documentation Paper. *Met Office*, 135-198.

[3] Lean, H.W., Clark, P.A., Dixon, M., *et al.* (2008) Characteristics of High-Resolution Versions of the Met Office Unified Model for Forecasting Convection over the United Kingdom. *Monthly Weather Review*, **136**, 3408-3424. https://doi.org/10.1175/2008MWR2332.1

[4] Gao. Y., Fu. J.S., Drake, J.B., Liu, Y. and Lamarque, J.F. (2012) Projected Changes of Extreme Weather Events in the Eastern United States Based on a High Resolution Climate Modeling System. *Environmental Research Letters*, **7**, Article 044025. https://dx.doi.org/10.1088/1748-9326/7/4/044025

[5] Latt, M.R., Hochman, A., Caldas-Alvarez, A., Helgert, S., Pinto, J.G. and Corsmeier,

U. (2022) Understanding Summer wind Systems over the Eastern Mediterranean in a High-Resolution Climate Simulation. *International Journal of Climatology*, **42**, 8112-8131. https://doi.org/10.1002/joc.7695

[6] Chen, W., Zhang, Y., Gao, W. and Zhou, D. (2016) The Investigation of Urbanization and Urban Heat Island in Beijing Based on Remote Sensing. *Procedia-Social and Behavioral Sciences*, **216**, 141-150. https://doi.org/10.1016/j.sbspro.2015.12.019

[7] De Meij, A., Zittis, G. and Christoudias, T. (2019) On the Uncertainties Introduced by Land Cover Data in High-Resolution Regional Simulations. *Meteorology and Atmospheric Physics*, **131**, 1213-1223. https://doi.org/10.1007/s00703-018-0632-3.

[8] Chen, Z.T., Xu, D.S., Dai, G.F., Zhang, Y.X., Zhong, S.X. and Huang, Y.Y. (2020) Technical Scheme and Operational System of Tropical High-Resolution Model (TRAMS-V3.0). *Journal of Tropical Meteorology*, **36**, 444-454. (in Chinese)

[9] Poschlod, B. (2021) Using High-Resolution Regional Climate Models to Estimate Return Levels of Daily Extreme Precipitation over Bavaria. *Natural Hazards and Earth System Sciences*, **21**, 3573-3598. https://doi.org/10.5194/nhess-21-3573-2021

[10] Mohanty, S., Nadimpalli, R., Mohanty, U.C., *et al.* (2021) Quasi-Operational Forecast Guidance of Extremely Severe Cyclonic Storm Fani over the Bay of Bengal Using High-Resolution Mesoscale Models. *Meteorology and Atmospheric Physics*, **133**, 331-348. https://doi.org/10.1007/s00703-020-00751-4

[11] Lin, X.X., Feng, Y.R., Chen, Z.T. and Jian, Y.T. (2021) Preliminary Evaluation of Forecast Skill of GRAPES GuangZhou Regional Modeling System. *Journal of Tropical Meteorology*, **37**, 656-668. (in Chinese)

[12] Zhou, Q. and Tong, C. (2022) Does Rapid Urbanization Improve Green Water-Use Efficiency? Based on the Investigation of Guangdong Province, China. *Sustainability*, **14**, Article 7481. https://doi.org/10.3390/su14127481

[13] Zhong, R., Song, S., Zhang, J. and Ye, Z. (2023) Spatial-Temporal Variation and Temperature Effect of Urbanization in Guangdong Province from 1951 to 2018. *Environment, Development and Sustainability*, 1-23. https://doi.org/10.1007/s10668-023-03113-3

[14] Ran, Y.H. and Li, X. (2015) First Comprehensive Fine-Resolution Global Land Cover Map in the World from China—Comments on Global Land Cover Map at 30- m Resolution. *Science China Earth Sciences*, **58**, 1677-1678. https://doi.org/10.1007/s11430-015-5132-4

[15] Jokar Arsanjani, J., See, L. and Tayyebi, A. (2016) Assessing the Suitability of GlobeLand30 for Mapping Land Cover in Germany. *International Journal of Digital Earth*, **9**, 873-891. https://doi.org/10.1080/17538947.2016.1151956